Intramolecular Charge Separation and Transition State Dynamics in Anthracene/ Pyridinium Supermolecules

T. Hirsch, H. Port,* and H. C. Wolf

3.Physikalisches Institut, Universität Stuttgart, Pfaffenwaldring 57, D-70550 Stuttgart, Germany

B. Miehlich and F. Effenberger

Institut für Organische Chemie und Isotopenforschung, Universität Stuttgart, Pfaffenwaldring 55, D-70550 Stuttgart, Germany

Received: December 3, 1996; In Final Form: March 24, 1997[⊗]

The excited state dynamics of anthracene (donor) and pyridinium or pyridine (acceptor) composed supermolecules has been studied applying femtosecond transient absorption and picosecond time-resolved fluorescence techniques. From the analysis of spectral and temporal dynamics of σ- and π-bridged systems **1a**−**4a**, the effects of molecular structure and environment on intramolecular charge separation in the excited state are differentiated. Two-step charge separation has been verified to occur for **2a** and **3a** in liquid environment by identifying neutral and radical ion states of the anthracene moiety on the sub picosecond time scale. Instead, after changing the substitution position of the acceptor to 3-pyridinium, charge separation does not occur. From evaluating the transient state dynamics in solvents of different polarity, rates for charge separation and relaxation can be quantified in terms of Marcus theory.

Introduction

Intramolecular charge separation in supermolecules containing various molecular subunits is of high interest when considering functionalized molecular materials.[1] Besides other intramolecular transfer mechanisms, already investigated,[2,3] charge separation in the photoexcited state has been explored on covalently linked model systems for photosynthesis[4] and on artificial model systems for a general understanding of charge separation and to improve its efficency.[5−8] Different dependencies of charge separation and recombination rates on the geometrical structure, the distance between electron donor and acceptor, and the molecular environment as well have been observed experimentally and were studied theoretically.[9−12] Thereby the rate of intramolecular charge separation and recombination is expected to show a remarkable dependence on solvent polarity, varying from values smaller than 1 ps to more than several 10 ns, predicted by electron transfer theory.[13−16]

In this paper, we are concerned with the electronic properties of acceptor-substituted anthracene supermolecules and the feasibility of charge separation in the optically excited state depending on the molecular composition. We have studied 4-(9-anthrylmethyl)-*N*-methylpyridinium tetrafluoroborate (**2a**)[17] as well as the systems **3a** and **4a**, the structures of which are derived from **2a** by extending the methylene σ-bridge with a vinylene unit and by varying the linkage position of the pyridinium acceptor (Figure 1).

Transient absorption in the subpicosecond time regime and time-resolved single photon counting techniques were combined to extend our knowledge of intramolecular charge separation which has been already proved for **2a**[18] by identification of an anthracene radical cation $\mathbf{A}^{\bullet+}$ in the excited state. Now, the dynamics of charge separation and recombination are investigated in solvents of different polarity and on molecules where the molecular structure is varied between different acceptor substitution positions, both 3-pyridinium and 4-pyridinium substitution (as in **2a**). The essential dynamical properties will be analyzed according to the reaction scheme in Figure 2. Within this picture the locally excited state (D*−A) is considered as possible precursor of the actual charge separation step towards $(D^+-A^-)^*$, whose rates of formation and recombination are denoted as k_{CS} and k_{CR}, respectively.

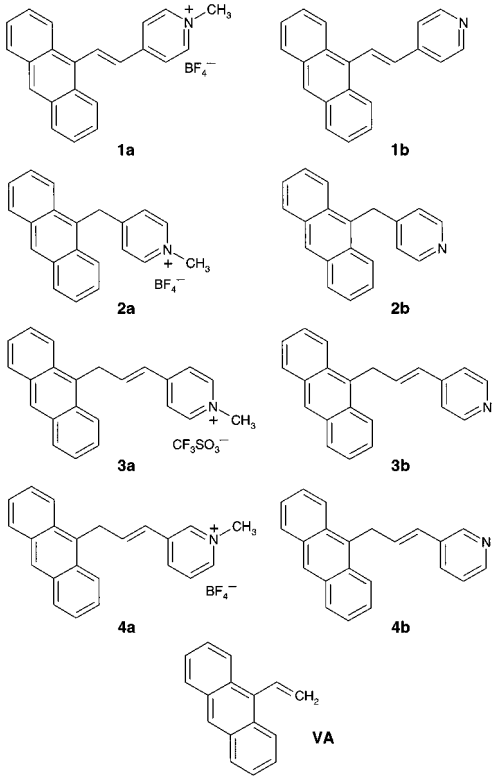

Figure 1. Molecular structure of the compounds investigated in the present study and of reference compound 9-vinylanthracene (**VA**).

Experimental Section

Synthesis of Compounds 3a,b and 4a,b. Uncorrected melting points were obtained with a Büchi SMP 20 apparatus.

* To whom correspondence should be addressed.

[⊗] Abstract published in *Advance ACS Abstracts,* May 1, 1997.

S1089-5647(96)03967-3 CCC: $14.00

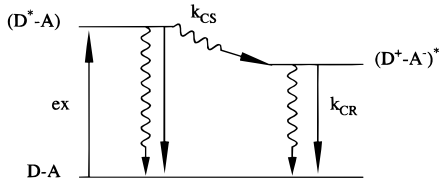

Figure 2. Kinetic scheme of photoinduced charge separation in a donor (D)−acceptor (A) supermolecule: groundstate (D−A), locally excited (D*−A), and charge-separated transient state $(D^+-A^-)^*$.

^{1}H NMR spectra were recorded at 250 MHz on a Bruker AC 250 F spectrometer; chemical shifts (δ values) are given in ppm relative to TMS as internal standard. Preparative column chromatography was performed using glass columns of different size packed with silica gel S, grain size 0.032−0.063 mm (Riedel−de Haën) or aluminum oxide. The synthesis of compounds **1a,b** and **2a,b** has been published previously.[17]

4-[3-(9-Anthryl)propenyl]pyridine (3b). At room temperature 1 mL (1.6 mmol) of *n*-BuLi in hexane (1.6 M) was added via syringe to 499 mg (1.7 mmol) of diphenyl-4-pyridylmethylphosphine oxide[19] in 1 mL of THF under argon atmosphere, and after 15 min 330 mg (1.5 mmol) of 9-anthrylacetaldehyde in 10 mL of dichloromethane was added dropwise within 1 h. The reaction mixture was stirred for 16 h, and the precipitated lithium phosphinate was carefully filtered off. The filtrate was concentrated, and crude **3b** was chromatographed on Al_2O_3 with dichloromethane as eluent and purified by recrystallization from ethanol: yield, 233 mg (53%); melting point, 146−147 °C. Anal. Calcd for $C_{22}H_{17}N$: C 89.46, H 5.80, N 4.74. Found: C 89.52, H 5.90, N 4.58. ^{1}H NMR ($CDCl_3$) δ 4.56 (dd, J_1 = 1.8, J_2 = 5.9 Hz, 2 H); 6.23 (d, J = 15.9 Hz, 1 H); 6.84 (dt, J_1 = 15.9, J_2 = 5.9 Hz, 1 H); 7.09 (d, J = 6.1 Hz, 2 H); 7.45−7.57 (m, 4 H); 8.05 (m_c, 2 H); 8.42 (m_c, 3 H).

4-[3-(9-Anthryl)propenyl]-1-methylpyridinium Trifluoromethanesulfonate (3a). 5 μL (0.44 mmol) of methyl trifluoromethanesulfonate was added via syringe at 0 °C to 88.6 mg (0.3 mmol) of **3b** in 1 mL of dichloromethane under argon atmosphere, and the reaction mixture was stirred for 30 min at room temperature in the absence of light. The resulting light yellow precipitate was collected by filtration under inert gas, washed with cold dichloromethane and diethyl ether, and dried under high vacuum: yield, 91.2 mg (59%) yellow powder. Anal. Calcd for $C_{24}H_{20}F_3NO_3S\cdot 0.667CH_2Cl_2$: C 57.40, H 4.17, N 2.71, S 6.21. Found: C 57.41, H 4.10, N 2.60, S 6.25. ^{1}H NMR (DMSO-d_6) δ 4.17 (s, 3 H); 4.72 (d, J = 6.2 Hz, 2 H); 6.65 (d, J = 15.9 Hz, 1 H); 7.45 (dt, J_1 = 15.9, J_2 = 6.2 Hz, 1 H); 7.58 (m_c, 4 H); 8.02 (d, J = 6.8 Hz, 2 H); 8.14 (m_c, 2 H); 8.37 (m_c, 2 H); 8.61 (s, 1 H), 8.72 (d, J = 6.8 Hz, 2 H).

3-[3-(9-Anthryl)propenyl]pyridine (4b). At 0 °C 1 mL (1.6 mmol) of *n*-BuLi in hexane (1.6 M) was added via syringe within 5 min to 499 mg (1.7 mmol) of diphenyl-3-pyridylmethylphosphine oxide[20] in 200 mL of THF under argon atmosphere, and after 40 min 330 mg (1.5 mmol) of 9-anthrylacetaldehyde in 15 mL of dichloromethane was added dropwise within 1 h. The reaction mixture was stirred for 42 h at room temperature, and the precipitated lithium phosphinate was carefully filtered off. The filtrate was concentrated in vacuo, and crude **4b** chromatographed twice on silica gel with 98:2 dichloromethane/methanol as eluent and purified by recrystallization from diisopropyl ether: yield, 173 mg (49%) yellow needles; melting point, 99−100 °C. Anal. Calcd for $C_{22}H_{17}N$: C 89.46, H 5.80, N 4.74. Found: C 89.55, H 5.88, N 4.08. ^{1}H NMR ($CDCl_3$) δ 4.54 (dd, J_1 = 1.6, J_2 = 5.8 Hz, 2 H); 6.29 (d, J = 16 Hz, 1 H); 6.66 (dt, J_1 = 16, J_2 = 5.8 Hz, 1 H); 7.11 (dd, J_1 = 7.9, J_2 = 4.8 Hz, 1 H); 7.45−7.56 (m, 5 H); 8.04 (m_c, 2 H); 8.25 (m_c, 2 H); 8.36 (d, J = 4.8 Hz, 1 H); 8.42 (s, 1 H); 8.45 (d, J = 1.7 Hz, 1 H).

3-[3-(9-Anthryl)propenyl]-1-methylpyridinium Tetrafluoroborate (4a). 68.3 mg (0.23 mmol) of **4b** in 8 mL of dichloromethane was added via syringe at 0 °C to 35 mg (0.24 mmol) of trimethyloxonium tetrafluoroborate in 10 mL of dichloromethane. After stirring for 2.5 h at room temperature in the absence of light, 1 mL of methanol was added to solvate the excess of oxonium salt. The solvent was removed, and the resulting precipitate was purified by recrystallizing twice from methanol: yield, 38.4 mg (42%) light yellow needles; melting point, 191.5−192.5 °C. Anal. Calcd for $C_{23}H_{20}BF_4N$: C 69.55, H 5.07, N 3.53. Found: C 69.41, H 5.07, N 3.38. ^{1}H NMR (DMSO-d_6) δ 4.18 (s, 3 H); 4.67 (d, J = 6.1 Hz, 2 H); 6.50 (d, J = 16.0 Hz, 1 H); 7.11 (dt, J_1 = 16.0, J_2 = 6.1 Hz, 1 H); 7.57 (m_c, 4 H); 7.96 (dd, J_1 = 8.2, $J2$ = 6.0 Hz, 1 H); 8.14 (m_c, 2 H); 8.37 (m_c, 2 H); 8.56 (d, J = 8.3 Hz, 1 H); 8.60 (s, 1 H); 8.71 (d, J = 6. 0 Hz); 8.93 (s, 1 H).

Anthracene **A** and 9-vinylanthracene **VA** used as reference compounds were obtained from Merck/Darmstadt and were used without further purification.

The solvents acetonitrile, THF, 1,2-dichloromethane, 1,2-dichloroethane (all Merck, UVASOL), butyronitrile, propionitrile, and valeronitrile (all Merck, synthesis grade) were used as purchased. 2-MTHF (Aldrich) was distilled and dried over elementary sodium. All measurements were performed in liquid solution at concentrations between 10^{-5} and 10^{-4} mol/L. The samples were degassed by repeated freeze−pump−thaw cycles.

Spectroscopic Methods. The absorption spectra at room temperature were recorded with a Perkin Elmer Lambda 16 UV/VIS spectrometer. Time-resolved fluorescence spectra were measured using the time-correlated single photon counting technique. The excitation source is a Nd:YAG synchronously pumped and frequency doubled picosecond dye laser providing picosecond pulses at 27 500 cm^{-1} at a repetition rate of 3.8 MHz. The system response time of the detection system is 30 ps. For further description see ref 3.

Measurements of transient absorption spectra and transients on femtosecond time scale were performed using two-pulse pump and probe technique. The basic laser source is a Nd:YLF pumped Ti:sapphire regenerative amplifier seeded at 25 000 cm^{-1} with a Kerr Lense mode-locked Ti:sapphire oscillator. The amplified pulses were determined to 180 fs (fwhm) with a pulse energy of >300 μJ at 1 kHz rate. The pump pulses were obtained by frequency doubling 20% of the amplified output within a 1.5 mm LBO crystal. The residual 80% were guided through an adjustable optical delay line and focused on a fast-rotating 5 mm quartz plate to generate the probe white light continuum. The probe light was split into two beams which were focused separately on the excited and nonexcited sample volume. A polychromator diffracted the two transmitted beams in signal and reference spectra which were recorded simultaneously by a dual-line photodiode array for each excitation pulse at 1 kHz repetition rate. The transient absorption spectra represent the ratio of reference (T) and signal ($T + \Delta T$) spectra corrected according the spectral response. The system response time was determined to be ~300 fs.

Special care was provided to take into account the temporal dispersion (chirp) of the white-light continuum. The dispersion was determined by inverse Raman[21,22] measurements of a mixture of different solvents correcting the transient spectra accordingly.

For both time-resolved methods a fitted model function of the transients was convoluted with the response function of the system.

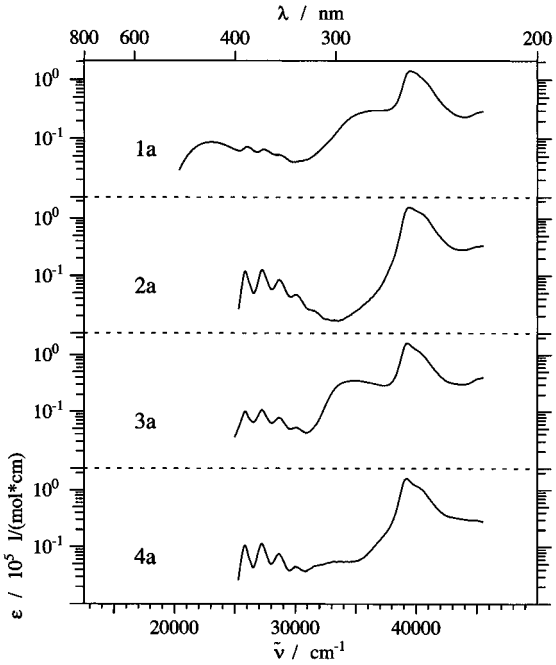

Figure 3. CW absorption spectra of the pyridinium-substituted compounds **1a**, **2a**, **3a**, and **4a** in acetonitrile at room temperature; extinction ϵ in logarithmic scale.

Results and Discussion

CW Absorption. The CW absorption spectra for the compounds **1a**−**4a**, **1b**−**4b**, **A**, and **VA** at $T = 300$ K are given in Figures 3 and 4. All pyridinium and pyridine substituted molecules exhibit an absorption band of reasonably high extinction ($\epsilon \sim 10^5$ L/(mol·cm) in the UV region at 39 000 cm^{-1} commonly classified as $S_3 \leftarrow S_0$ transition of the anthracene moiety.[23] Additionally, a low-energy absorption at 25 900 cm^{-1} with a pronounced vibronic structure is present for the σ-bridged systems **2a**−**4a** and **2b**−**4b** corresponding to the $S_1 \leftarrow S_0$ transition of the anthracene moiety,[23] however, due to the substitution shifted by about ∼800 cm^{-1} to the red. In compounds **2a**−**4a** and **2b**−**4b** the anthracene clearly dominates the low-energy absorption allowing for selected excitation of the donor moiety in the supermolecule.

For the π-bridged systems **1a** and **1b** the vibronic substructure of the anthracene $S_1 \leftarrow S_0$ band is effectively diminished in favor of another unstructured low-energy absorption with maximum at 23 000 and 26 000 cm^{-1}, respectively. This additional transition cannot be related to an individual molecular subunit or the 9-vinylanthryl group **VA**. It might be interpreted as an optical partial charge separation because the redox potentials of anthracene ($E_{ox} = +1.09$ eV) and pyridinium ($E_{red} = -1.21$ eV)[24] meet the requirement for a charge separation transition in the excited state of **1a**. This can be estimated from the exergonic stabilization energy $\Delta G = -4440$ cm^{-1} relative to the energy $E_{ex} = 23\,000$ cm^{-1} of the photoexcited state. The value of ΔG was calculated according to the Rehm−Weller equation[25] $\Delta G = E_{ox} - E_{red} - E_{ex}$ neglecting the Coulomb part of the stabilization energy. The results on **1a**, and **1b** are discussed in more detail in the context of molecules with elongated polyene chain.[12,18,26]

The absorption spectra of **1a**, **3a**, and **4a** exemplify another effect related to the substitution position of the donor pyridinium. For **1a** and **3a** (Figure 1), with the pyridinium substituted to the vinyl group in 4-position, an additional broad absorption band at ∼34 000 cm^{-1} is observed (Figure 3). In contrast, for **4a** substituted with the pyridinium in the 3-position this transition vanishes almost completely. Apparently the strength of the coupling between the vinyl and pyridinium moieties is heavily influenced by the substitution position. The coupling strength is correlated with the higher electron density of pyridinium at the 4-position ($\rho = 0.369$) as compared to that at the 3-position ($\rho = 0.046$).[27,28] Consequently, the observed transition at 34 000 cm^{-1} in **1a** and **3a** is attributed to the vinylpyridinium subunit.

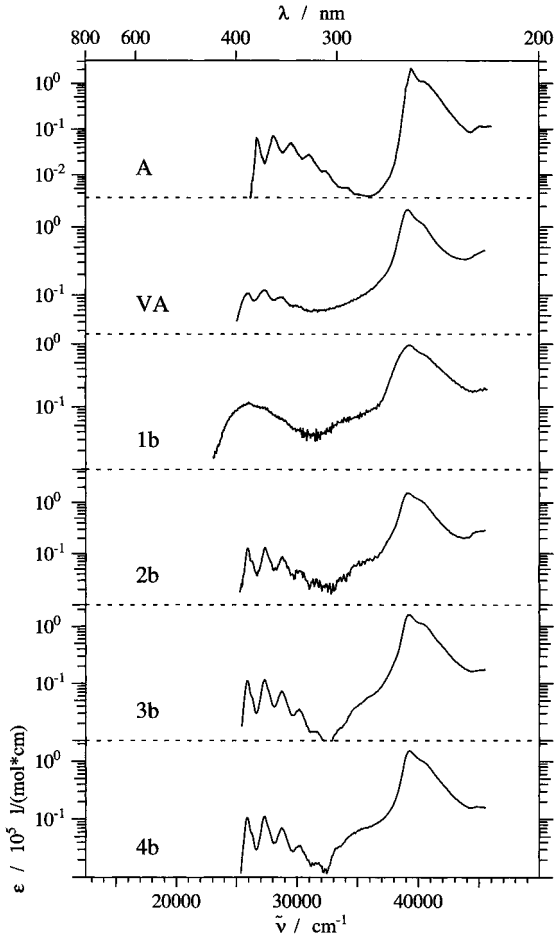

Figure 4. CW absorption spectra of **A** and **VA** and of the pyridine-substituted compounds **1b**, **2b**, **3b**, and **4b** in *n*-hexane at room temperature; extinction ϵ in logarithmic scale.

Transient Absorption: Evidence for Charge Separation. The transient absorption measurements were made with the intention to prove intramolecular charge separation in **1a**−**4a**. The identification of charge separation was carried out by comparison of the spectra with the spectra of the respective radical cation. Its dynamics was determined by transients measured at selected detection energies. The compounds **1b**−**4b**, **A**, and **VA** are used for reference to identify the excited donor without relaxation into an ionic state and to separate contributions from charge separation and molecular geometry.

As an example, the transient spectra of **2a** in acetonitrile, Figure 5, are recorded in successive time intervals of 100 fs before and after pulse excitation at 25 000 cm^{-1}. The main features are two absorption subspectra ($T/T + \Delta T$) > 1) with maxima at 17 100 and 14 100 cm^{-1} evolving on short and longer time scales, respectively. As discussed in more detail below, the two transient spectral components extracted from Figure 5 (see Figure 8) are in good agreement with the calculated excited state singlet−singlet absorption of neutral anthracene ($S_7 \leftarrow S_1$)[29] and with the absorption spectra of an anthracene radical cation, $\mathbf{A}^{\bullet+}$.[30,31]

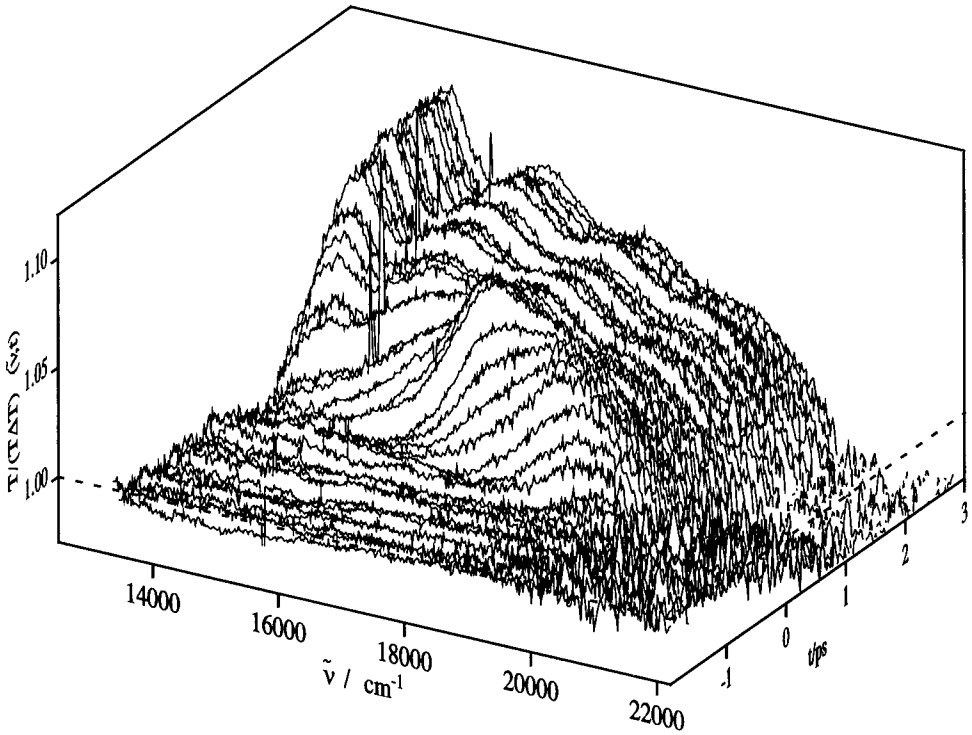

Figure 5. Transient absorption spectra of the pyridium-substituted compound **2a** in acetonitrile at room temperature, not corrected for the chirp of the white light. Successive spectra were recorded in intervals of 100 fs.

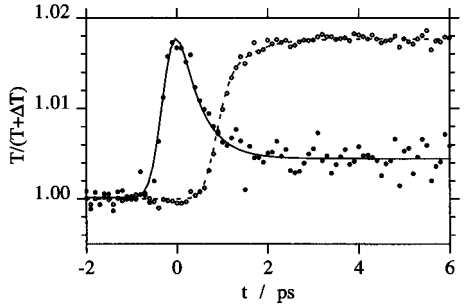

Figure 6. Corresponding transients of **2a** in acetonitrile detected at 17 100 cm^{-1} (●) and 14 100 cm^{-1} (○), respectively, normalized to maximum intensities. Exponential curve fitting gives a decay time τ_1 = 490 fs (—) and a rise time τ_2 = 560 fs (- - -).

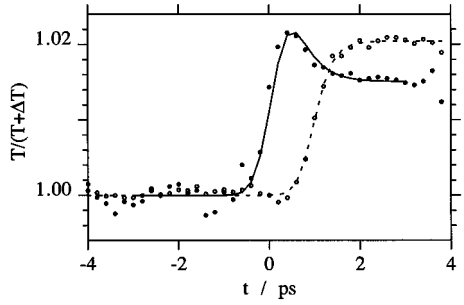

Figure 7. Corresponding transients of **3a** in acetonitrile detected at 17 200 cm^{-1} (●) and 14 300 cm^{-1} (○), respectively, normalized to maximum intensities. Full (—) and dotted lines (- - -) represent exponential curve fitting.

The corresponding individual transients of **2a** recorded at 17 100 and 14 100 cm^{-1}, respectively, in steps of 100 fs are presented in Figure 6. Deconvolution of the data with the response function of the experimental setup yields exponentials as best fits. The fast high-energy component at 17 100 cm^{-1}, in the following denoted **B**, has a decay time of $\tau_1 = 490 \pm 50$ fs and is attributed to the decay of the primary excited S_1 state of anthracene. The rise time $\tau_2 = 560 \pm 50$ fs of the low-energy component at 14 100 cm^{-1} in the following denoted **A** is attributed to the fast buildup of the anthracene radical cation state. An additional slow decay component with $\tau_3 = 1.0 \pm 0.1$ ns contained in both transients is attributed to the lifetime of the charge−separated state. Within the experimental error the time constants τ_1 and τ_2 are equal. Obviously, the transients of **B** and **A** (decay and buildup) are coupled dynamically, representing charge separation at a time scale of $\tau_{CS} \sim \tau_1 \sim \tau_2$. It is concluded that charge separation occurs in two steps; the S_1 state of the anthracene moiety is the precursor state of the charge-separated state of the supermolecule.

Upon extending the type of bridge from methyl in **2a** to methylvinyl in **3a** spectral characteristics and dynamics in transient absorption remain very similar. Figure 8 displays the transient absorption spectra of **3a** observed at ∼300 fs and ∼2 ps after pulse excitation, respectively, appropriately corrected for the chirp of the white light probe beam. The two subspectra of the methylvinyl-separated compound **3a** appear in the same energy range as those of **2a** described above. For **3a** the spectrum in the region of 17 000 cm^{-1} is equally attributed to the neutral state and the spectrum in the region of 14 000 cm^{-1} to the radical state of the anthracene moiety. Individual transients measured at 17 200 and 14 300 cm^{-1} (Figure 7) prove the coupled dynamics with corresponding decay time of the neutral state and rise time of the radical state (Table 1). Consequently, charge separation proceeds in the same time range as for **2a** from the locally excited state of anthracene. In contrast, the decay time of the radical state at ∼14 000 cm^{-1} decreases within a factor of 21 as compared to **2a**. This effect is attributed to the vinyl group enhancing nonradiative decay channels.

For **4a** the molecular constitution is not changed as compared to **3a** but the pyridinium substitution position is turned to the 3-position. The transient absorption measurements reveal two dynamically coupled absorption bands. The absorption band with maximum at 17 200 cm^{-1} is comparable with the high-energy bands B of **2a** and **3a** (see Figure 8) and is therefore attributed to the locally excited state of the anthracene subunit.

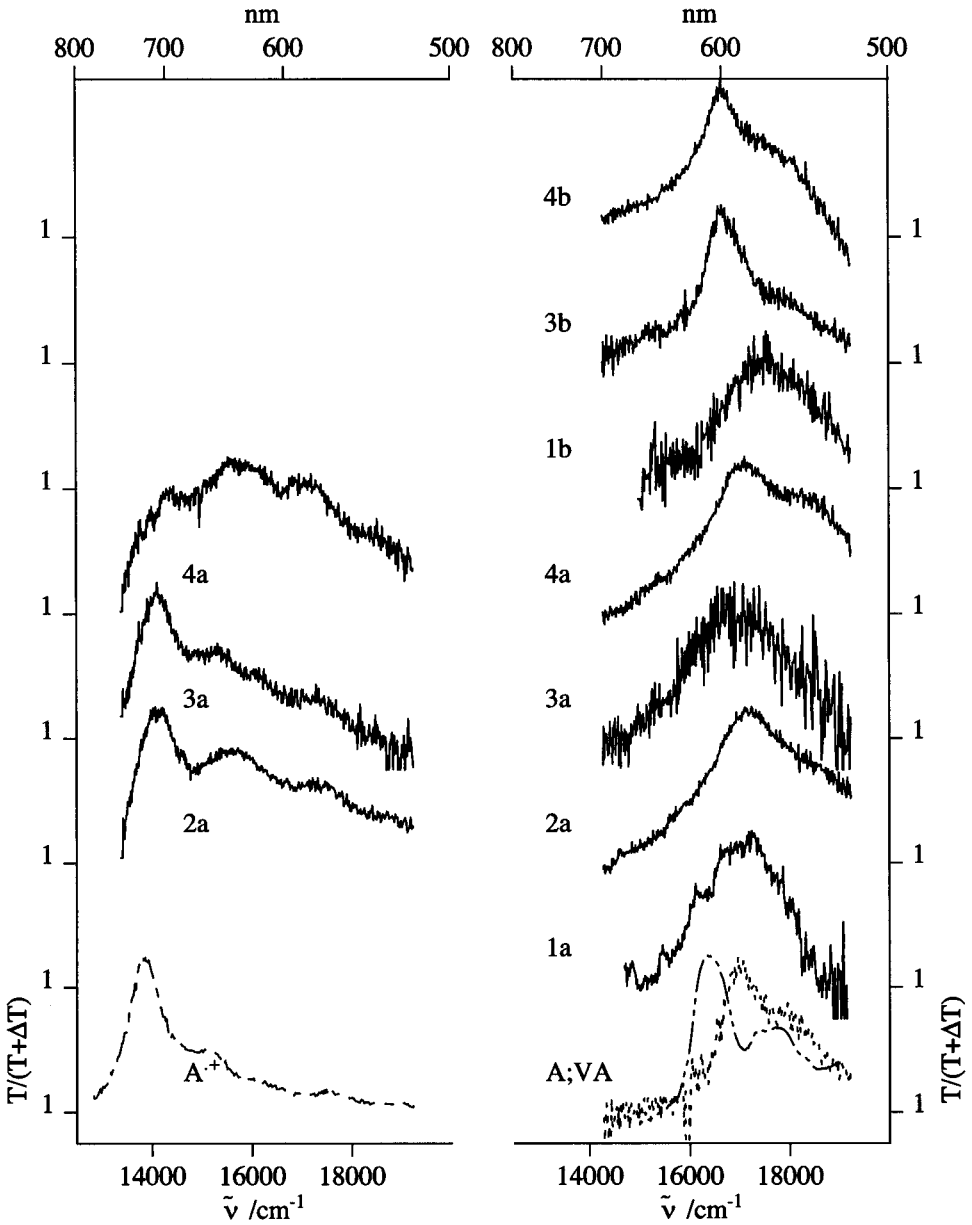

Figure 8. Transient absorption spectra of **1a**−**4a**, **1b**, **3b**, and **4b** at ∼300 fs (right, B bands) and ∼2 ps (left, A bands) after pulse excitation at 400 nm. Broken lines denote the absorption spectra of an anthracene radical ion $A^{\bullet+}$ (-−-−-)[30,31] and the transient absorption spectra of **A** (--−--−)[29] and **VA** (- - -) used as reference. (The spectra are corrected with respect to the chirp contained in the probe white light continuum and normalized to equal maximum intensity.)

As time progresses, the absorbance decreases with a time constant of 1.5 ps and correspondingly another broad absorption band with maximum at 15 700 cm^{-1} is built up at the same time scale ($\tau_1 \sim \tau_2$; see Table 1). However, the low-energy absorption of **4a** does not correspond to the anthracene cation identified in the excited state spectra of **2a** and **3a** (bands B; Figure 8). Therefore, the low-energy transient absorption of **4a** tentatively is attributed to a less polarized state compared to **2a** and **3a**. Presumably, it results from the reduced coupling of the subunits of **4a** not allowing for charge separation.

In contrast to the σ-bridged systems **2a** and **3a**, no anthracene radical cation has been detected for the π-bridged system **1a**. The transient absorption measurements yields a single high-energy transient band dominated by the neutral anthracene moiety (Figure 8). From the CW absorption experiments and semiempirical calculations on anthracene-substituted polyenes,[12] it is evident that the donor, bridge, and acceptor moieties are strongly coupled. Consequently, free-radical formation is not to be expected. π-Bridges, however, do not exclude charge separation in general. In other donor−acceptor-substituted polyenes, charge separation has been observed.[5,6]

For the pyridine-substituted reference compounds **1b**, **3b**, and **4b** (Figures 8 and 9), a single transient absorption of the neutral donor was observed, which finding is in accord with the data reported in ref 29 (Figure 8, A). It can be concluded that the locally excited state of the donor is not essentially affected by both acceptor subunits, pyridine and pyridinium.

Solvent Dependence of the Charge Separation Rate. The solvent dependence of intramolecular charge separation has been studied in more detail for **2a**. Upon variation of the solvent polarity, the same spectral features as reported above have been found. The transient absorption measurements always yield two spectral components which are correlated dynamically. The low-energy absorption corresponds to the radical cation of the anthracene moiety (Figure 8). Its maximum position does not change with solvent (Figure 10), indicating that the transition energy also is not influenced by the solvent. Thereby, however, no distinction is possible from the case that the absolute energies

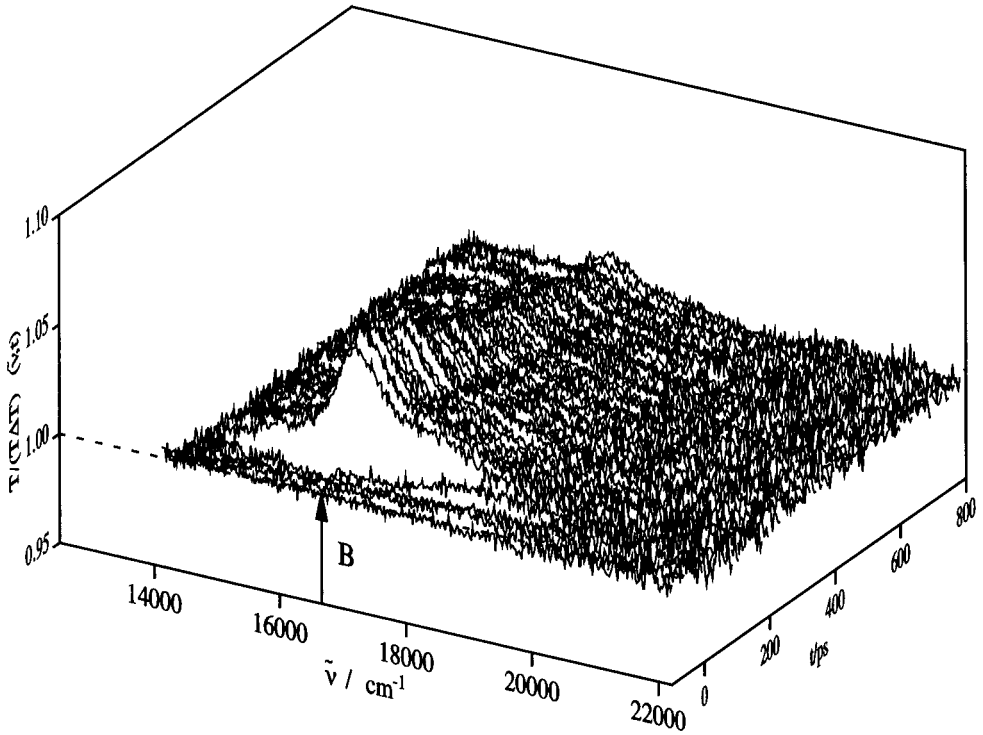

Figure 9. Transient absorption spectra of the pyridine-substituted compound **3b** measured in *n*-hexane at room temperature. The arrow marks the maximum position of transient absorption B.

TABLE 1: Decay and Rise Times of the Individual Transients of 1a−4a in Solvents with Different Dielectric Constants ϵ (Ref 43)[a]

sample	solvent	ϵ	τ_1/ps (±10%)	τ_2/ps (±10%)	τ_3/ns (±10%)
1a	acetonitrile	37.5	45		
2a	acetonitrile	37.5	0.49	0.56	1.02
	propionitrile	28.6	0.61	0.63	
	butyronitrile	22.3	0.57	0.53	1.36
	valeronitrile	19.4	0.58	0.37	1.42
	dichloroethane	10.6	≤1.0	0.38	
	dichloromethane	9.1	≤1.0	0.34	
	THF	7.4	0.71	0.65	
3a	acetonitrile	37.5	0.39	0.30	0.047
	butyronitrile	22.3	0.58	0.66	0.098
	valeronitrile	19.4	0.44	0.39	0.12
4a	acetonitrile	37.5	1.5	1.5	0.039
1b	*n*-hexane	1.9	530		
3b	*n*-hexane	1.9	520		
4b	*n*-hexane	1.9	340		

[a] τ_1 is the decay time of the high-energy component **B** of the transient absorption spectra. τ_2 and τ_3 are the rise and decay time of the low-energy component **A**. For **1b**, **3b**, and **4b** there was only one transient with the decay time τ_1 observed.

of the involved electronic states have been shifted equally in the same direction and thus these changes do not show up in the transient absorption measurement.

The dynamics of the intramolecular charge separation does not vary drastically but clearly depends on the solvent used. The decay time of the neutral excited state of the donor and correspondingly the rise time of the radical cation are prolonged from $\tau_1 = 490$ fs in acetonitrile to $\tau_1 = 710$ fs in THF (Table 1).

It follows that the rate of charge separation ($1/\tau_{cs} \sim 1/\tau_1 \sim 1/\tau_2$) actually is solvent dependent. In a first phenomenological approach (Figure 11), the values τ_{cs} are plotted as a function of the dielectric constant ϵ of the different solvents used and compared with dependencies of relaxation time constants characterizing these solvents: whereas both Debye relaxation

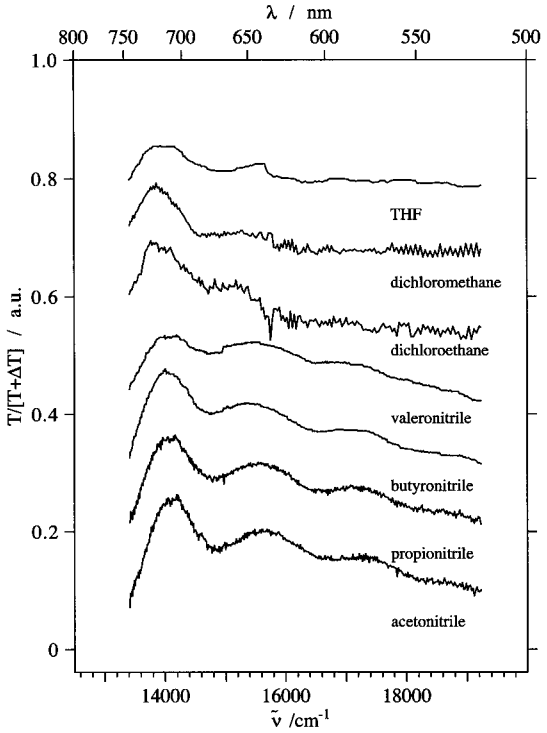

Figure 10. Transient absorption spectra of **2a** in different solvents. Low-energy component **A**, 2 ps after pulse excitation.

time τ_D and solvation time τ_S vary much stronger with ϵ, the values of the longitudinal relaxation time τ_L are comparable exhibiting a very similar weak dependence on ϵ. (τ_D and τ_L are also distinguished as constant field and constant charge relaxation times, respectively.[32,33]) This result suggests that the time scale of intramolecular charge separation is governed by τ_L, an essential contribution to the polarization relaxation of the solvent.[34] The proportionality $\tau_{CS} \sim \tau_L$ tentatively concluded from Figure 11, and also reported in refs 35 and 36, can be verified from theory for the present case and will be described

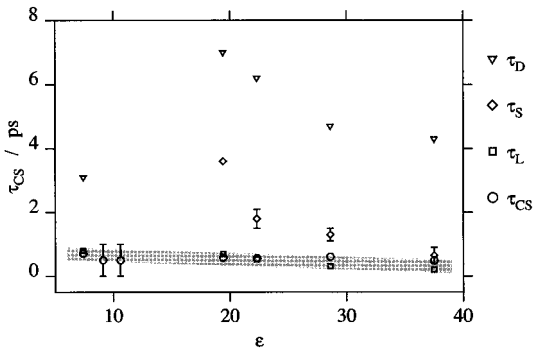

Figure 11. Charge separation time $\tau_{CS} \sim \tau_1 \sim \tau_2$ (see text) for **2a** measured in solvents with different dielectric constant ϵ. τ_L, τ_S, and τ_D[35,37] are the values of the corresponding longitudinal relaxation, solvation, and Debye relaxation times.

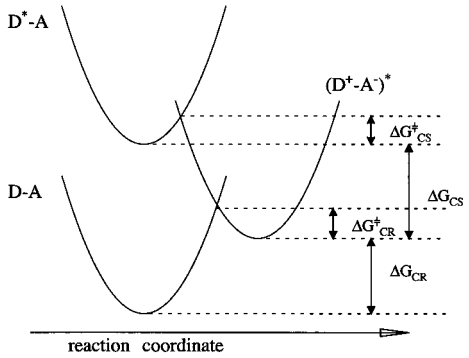

Figure 12. Basic parabola model of photoinduced electron transfer. $\Delta G^{\ddagger}$ and ΔG denote the energy barrier and the free energy, respectively, of electron transfer labeled CS and of relaxation labeled CR.

briefly in the following. The rate of charge separation $k_{CS} = 1/\tau_{CS}$ can be discussed in a reaction scheme commonly used (Figure 12) where ΔG denotes the free energy of the reaction. According to the Marcus theory k_{CS} is exponentially dependent on the reaction barrier $\Delta G^{\ddagger}$:

$$k_{CS} = a \exp(-\Delta G^{\ddagger}/k_B T) \quad (1)$$

with $\Delta G^{\ddagger} = (\Delta G + \lambda)^2/4\lambda$; k_B is the Boltzmann constant, and a is the preexponential factor generally representing the electronic and nuclear factors. The free energy for charge separation ΔG_{CS} can be calculated according to refs 13−16, when treating the solvent as dielectric continuum and the molecular subunits as spheres and referring to the redox potentials of the donor and the acceptor measured in acetonitrile, $\epsilon = 37$:

$$\Delta G_{CS} = -E_{00}(D) + e(E_{ox}(D) - E_{re}(A)) - \frac{e^2}{\epsilon R_z} - \frac{e^2}{2}\left(\frac{1}{r_D} + \frac{1}{r_A}\right)\left(\frac{1}{37} - \frac{1}{\epsilon}\right) \quad (2)$$

For the compounds **2a** the standard spherical radii of $r_D = 3.81$ Å, $r_A = 3.39$ Å, and $R_z = 5.1$ Å (calculated applying AM1[18]) have been used in order to determine the ΔG_{CS} values listed in Table 2. As all values for the different solvents are negative, the basic requirements for charge separation are confirmed, and the reaction always processes exothermically, although a slight dependence of ΔG_{CS} on ϵ is found.

In principle, the dynamics of a specific solvent can be described by the Debye relaxation time τ_D, commonly associated with molecular motion, the solvation time τ_S, and the longitudinal relaxation time τ_L, related to τ_D by $\tau_L = \tau_D(\epsilon_\infty/\epsilon)$.[33−37] If polarization relaxation of the solvent in the limit of τ_L plays a dominant role for the charge separation reaction with a sufficiently high electronic coupling, the preexponential factor in eq 1 is reduced to $1/\tau_L$.

TABLE 2: Calculated Free Energy ΔG of Electron Transfer (ΔG_{CS}) and Recombination (ΔG_{CR}) for 2a in Solvents with Different Dielectric Constant ϵ and Solvent Reorganization Energy λ_s[a]

solvent	ϵ	ΔG_{CS}/eV	ΔG_{CR}/eV	λ_s/eV	τ_3/ns
acetonitrile	37.5	−0.977	−2.233	0.80	1.00
propionitrile	28.6	−0.964	−2.246	0.75	1.17
butyronitrile	22.3	−0.950	−2.260	0.76	1.37
valeronitrile	19.4	−0.940	−2.270	0.71	1.50
1,2-dichloroethane	10.6	−0.874	−2.336	0.59	2.38
1,2-dichloromethane	9.1	−0.850		0.59	
THF	7.4	−0.812		0.49	

[a] In the calculations a center to center distance of $R_c = 5.1$ Å and an ionic radius of 3.81 and 3.39 Å were employed. τ_3 is the lifetime of the low-energy fluorescence A of **2a** in the specified solvents. The lifetime τ_1 of the high-energy fluorescence B and the rise time τ_2 of A are faster than the response time of the experimental setup.

$$k_{CS} = \frac{1}{\tau_L} \exp\left(-\frac{\Delta G^{\ddagger}}{k_B T}\right) \sim \frac{1}{\tau_L} \quad (3)$$

With the values for the free energy ΔG_{CS} and the solvent relaxation energy λ_S, calculated in Table 2, the charge separation rate is dominated by the preexponential factor. The measured correlation of the charge separation rate with τ_L suggests that polarization relaxation of the solvent in the limit of τ_L plays a dominant role for intramolecular charge separation in **2a**. The influence of polarization relaxation in the time range of the first 100 fs could not be observed because of time resolution. Moreover, on this short time scale solvent relaxation can occur nonexponential or even Gaussian.[38,39] In contrast, simple continuum models predict that the polarization in solvents with one Debye constant τ_D has an exponential response.

The weak ϵ dependence and the measured correlation with τ_L reveals that the observed charge separation can be described by (3), similarly as reported in ref 40.

Time-Resolved Dual Fluorescence and Charge Recombination. Additionally, some aspects of the excited state dynamics have been deduced from time-resolved fluorescence measurements. While the charge separation reaction is too fast to be followed in emission, relaxation to the ground state can readily be analyzed in both fluorescence spectra and transients.

Figure 13 displays the time-resolved spectra of **2a** recorded in butyronitrile, as an example, at $T = 300$ K, in consecutive time intervals of 0−73 and 73−146 ps after picosecond pulse excitation in comparison with the quasi-stationary fluorescence spectra. At early times (0−73 ps) the fluorescence reveals a high- and a low-energy component, in correspondence to transient absorption measurements denoted B and A, with the maximum at 24 000 and 15 500 cm^{-1}, respectively, and a clearly resolved vibronic structure for B. At later times the unstructured band A predominates. From the anthracene-like energetic position and vibronic structure, B is attributed to the fluorescence of the locally excited anthracene moiety.

Individual transients of B and A fluorescences are also given in Figure 13. The decay time of B is faster than the response time of the detection system (<30 ps) as it is for the rise time of A. However, the decay of A is measurable and single exponential and depends on the solvent used. With decreasing values of the static dielectric constant ϵ, the fluorescence decay time of A increases from 1.00 ns (acetonitrile) to 2.38 ns (1,2-dichloroethane) (Table 2). (For several solvents listed in Table

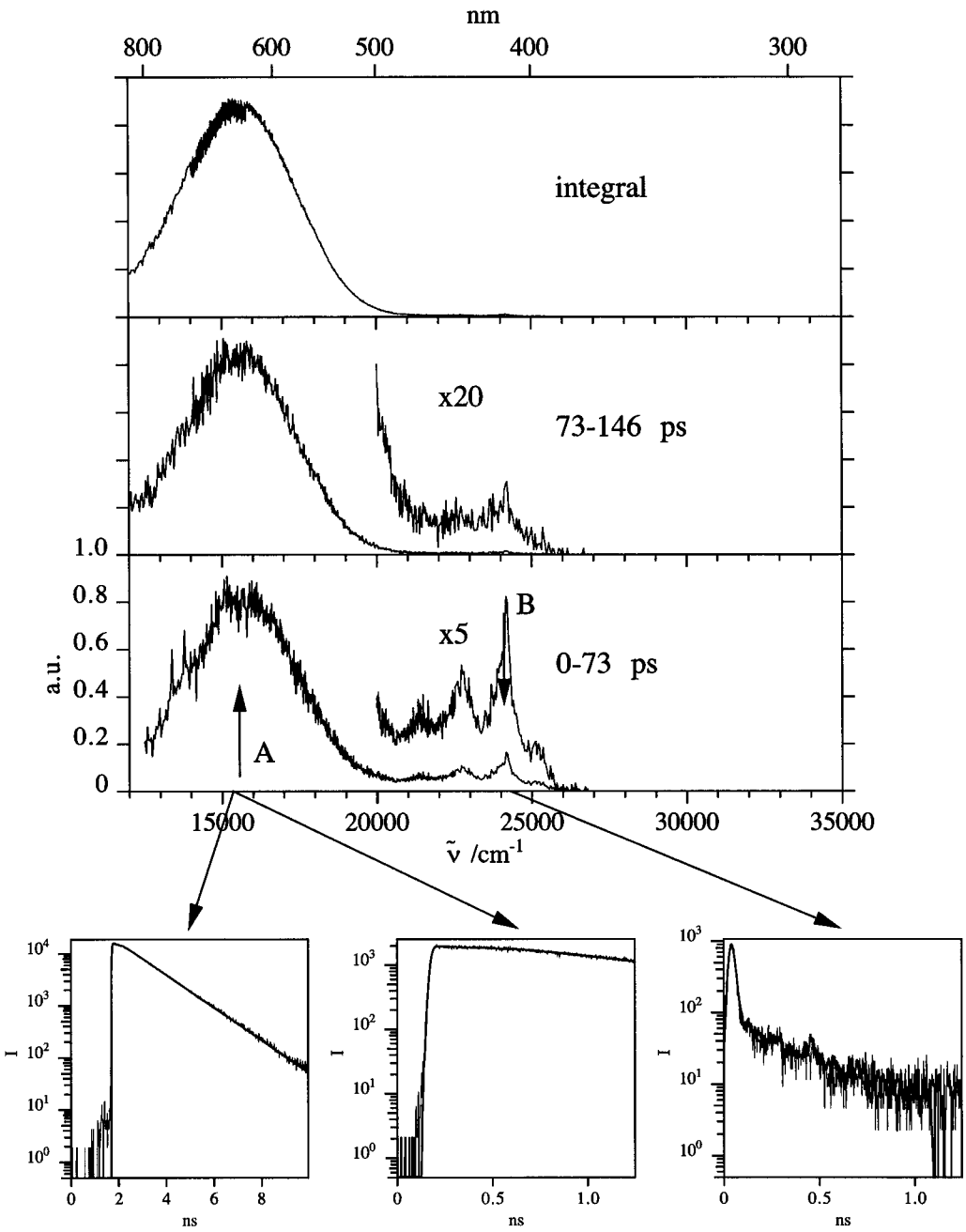

Figure 13. Time-resolved fluorescence of **2a** in butyronitrile at time intervals 0−73 and 73−146 ps after pulse excitation. Maxima position of low and high energy fluorescence components are marked A and B. Transients detected at different energies are displayed in logarithmic scale.

2, the decay time is not measurable because of very low fluorescence intensity due to poor solubility of the supermolecules.)

The decay time τ_3 of the B fluorescence (Table 2) and the decay time τ_3 deduced from low-energy region B of transient absorption (Table 1) are equal within the limits of error. This correspondence confirms the low-energy fluorescence component A to originate from the charge separated state $(D^+-A^-)^*$ and measures its recombination to the ground state (Figure 2). It will be shown below that a quantitative description of the relaxation rates can be given.

For supermolecule **3a** in which the bridge between donor and acceptor is enlarged, from $-CH_2-$ to $-CH_2-CH=CH-$, no fluorescence emission is observed at 300 K. Since charge separation in **3a** is as fast as in **2a**, measured by transient absorption, this finding indicates an enhanced nonradiative relaxation from the excited donor to the ground state. Actually those can be slowed down upon decreasing the environmental temperature. At $T = 140$ K, just above the glass point of MTHF, the time-resolved fluorescence becomes detectable (Figure 14). The spectra measured in different time intervals (0−40, 60−120, and 370−430 ps) reveal a large dynamical Stokes shift of about 4000 cm^{-1}. Moreover, at early times the high-energy portion of the spectrum exhibits two peaks at about 23 000 and 22 100 cm^{-1}, which are indicative for anthracene emission. On the other hand, the spectral position of the broad red-shifted band at long times is identical to the one observed in the fluorescence of **2a**. Thus the fluorescence spectra of compound **3a** also reflect the evolution in time from locally excited anthracene to the charge-separated state comparable with compound **2a**.

Upon further reduction of the temperature to 100 K the spectral dynamics remains qualitatively similar but evolves on longer time scales and with reduced overall red shift due to the increased rigidity of the solvent environment. Finally, at $T =$ 50 K only one fluorescence component is left over, which does

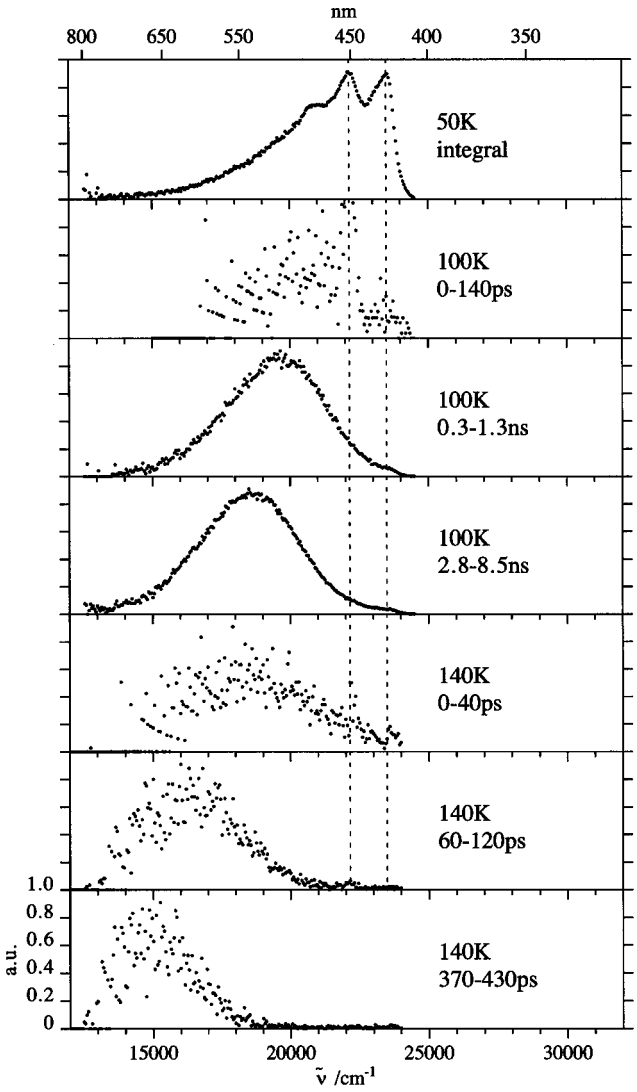

Figure 14. Time-resolved fluorescence of **3a** in 2-MTHF at $T = 140$, 100, 50 K, respectively, detected in different time intervals; the dotted lines (- - -) mark the energetic position of the (anthracene) fluorescence band at $T = 50$ K, as reference.

not evolve in time and whose energetic position and vibronic substructure correspond to anthracene. At this low temperature the intramolecular charge separation appears to be suppressed.

When the substitution position of the electron acceptor is varied from 4-pyridinium in **3a** to 3-pyridinium in **4a** the fluorescence behavior is drastically changed. Fluorescence becomes observable at $T = 300$ K like for **2a**, it consists, however, of a single high-energy component (Figure 15) only. No spectral dynamics is observed; the energetic position and vibronic substructure correspond to the anthracene-like **B** component of **2a** (Figure 13). On the other hand, the fluorescence decay time agrees with the decay time (τ_3) of the low-energy component in the transient absorption spectra of **4a** (Table 1). This means that the excited state probed in fluorescence and transient absorption measurements is the same belonging to the excited donor which before seems to undergo a electronic relaxation not observed in fluorescence measurement. Obviously no complete charge separation takes place in **4a**.

Model Description of the Recombination Rate. Within the framework of the model characterized in Figure 12 not only the rate of charge separation (see above) but also the recombination rate k_{CR} from the charge-separated state and its solvent dependence can be described quantitatively. The free energy for the relaxation to the ground state $(D^+-A^-)^* \rightarrow (D-A)$ is given by $\Delta G_{CR} = E_{00} + \Delta G_{CS}$ (Figure 12, Table 2). Thereby E_{00} is the excitation energy of the donor and $\Delta G^{\ddagger} = (\Delta G + \lambda)^2/4\lambda$ the reaction barrier,[13-15] similarly as in eq 1, including the total reorganization energy λ of the reaction. These observations indicate a weak solvent dependence of the energy gap ΔG_{CR} (Table 2). Thus, the measured decay rate k may be compared with the predictions of electron transfer theory. In the limit of both low temperature and strong electronic coupling the rate of charge separation or recombination can be written as follows:[41]

$$k = \frac{1}{\tau} = k_{rad} + \frac{|H_{el}|^2\sqrt{4\pi}}{\hbar(\lambda\hbar\langle\omega\rangle)^{1/2}} \exp\left(-\frac{2\Delta G^{\ddagger}}{\hbar\langle\omega\rangle}\right) \qquad (4)$$

where H_{el} is the electronic matrix element. Equation 4 is extended by including the radiative rate constant k_{rad} which also contributes to the overall rate k. The assumption of the low-temperature limit for k calculated with eq 4

$$\hbar\langle\omega\rangle/k_B T \gg 1 \qquad (5)$$

is satisfied as a mean vibrational frequency $\langle\omega\rangle = 1300$ cm^{-1} is calculated for **2a** applying AM1. The assumption of strong coupling limit requires

$$\lambda/\hbar\langle\omega\rangle \gg 1 \qquad (6)$$

with the total reorganization energy λ being larger than the solvent reorganization energy λ_s (eq 7), $\lambda \geq \lambda_S$:[42]

$$\lambda_s = -e^2\left(\frac{1}{2r_D^+} + \frac{1}{2r_A^-} - \frac{1}{R_z}\right)\left(\frac{1}{\epsilon} - \frac{1}{n^2}\right) \qquad (7)$$

The measured fluorescence decay rates k allow us to estimate from eq 4 the electronic matrix element $H_{el} = 100$ cm^{-1} and a total reorganization energy of $\lambda = 6760$ cm^{-1} with the radiative rate constant $k_{rad} = 1/4.9$ ns^{-1}. Figure 16 represents the experimental data and the theoretical curve calculated from eq 4. These values classify the relaxation of the excited charge-separated state to the ground state consistently to the strong electronic coupling limit ($H_{el} > 1$ cm^{-1}) in the inverted region with $\lambda < -\Delta G_{CR}$. Moreover, for molecular systems in which donor and acceptor are linked by a nonconjugated bridge, comparable values of H_{el} and λ are reported in the literature.[11] Finally, in contrast to the charge separation, where the rate is determined by solvent motion, i.e., environmental interactions, charge recombination is mainly influenced by intrinsic molecular parameters.

Summary

The basic properties of intramolecular charge separation in derivatives of 4-(9-anthrylmethyl)-*N*-methylpyridinium tetrafluoroborate have been studied in liquid solution. Applying ultrafast transient absorption and time-resolved fluorescence techniques in the σ-bridged compounds **2a** and **3a**, charge separation has been identified as a two-step process via the initially photoexcited neutral anthracene to the anthracene radical cation on sub-picosecond time scale. Moreover, the dynamics of charge separation is mainly ascribed to the polarization relaxation τ_L of the solvent. Conversely, the relaxation rate of the radical state is several orders of magnitude slower than the charge separation. It has been modeled by intrinsic molecular parameters using electron transfer theory in the limit of low temperature and strong electronic coupling of the molecular

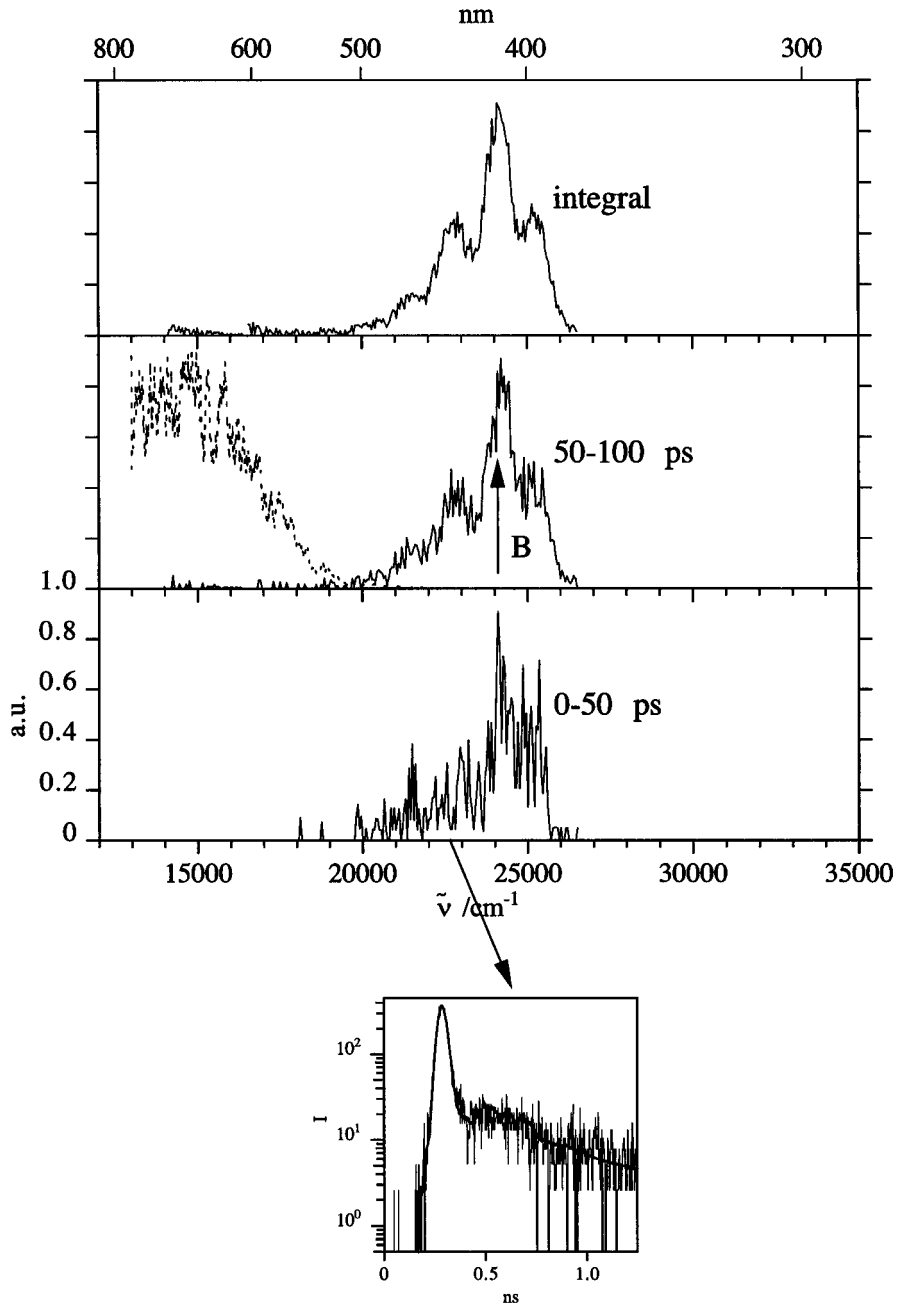

Figure 15. Time-resolved fluorescence band B of **4a** in acetonitrile at $T = 300$ K detected in time intervals 0−50 and 50−100 ps after pulse excitation. The fluorescence band A of **2a** in acetonitrile (- - -) is displayed for comparison. The transient is displayed in logarithmic intensity scale.

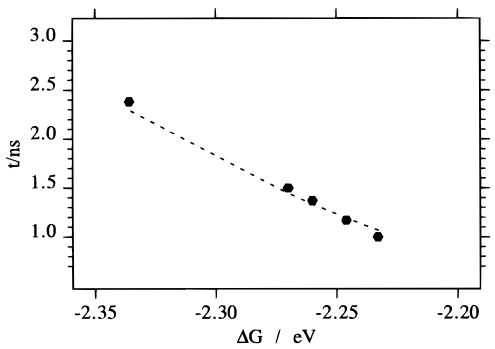

Figure 16. Fluorescence lifetime of **2a** measured in various solvents with different free energy ΔG_{CR}; broken line (- - -) calculated from eq 4.

moieties. A different behavior is observed especially for compound **4a** where the acceptor moiety is attached differently and the electronic coupling of the molecular subunits is reduced, and thus formation of an anthracene radical cation is suppressed.

Acknowledgment. We are grateful to the Deutsche Forschungsgemeinschaft, SFB 329, for financial support.

References and Notes

(1) Lehn, J.-M. *Ang. Chem., Int. Ed. Engl.* **1988**, *27*, 89.
(2) Holl, N.; Port, H.; Wolf, H. C.; Strobel, H.; Effenberger, F. *Chem. Phys.* **1993**, *176*, 215.
(3) Wiechmann, M.; Port, H.; Frey, W.; Lärmer, F.; Elsässer, T. *J. Phys. Chem.* **1991**, *95*, 1918.
(4) Macpherson, A. N.; Liddell, P. A.; Lin, S.; Noss, L.; Seely, G. R.; DeGraziano, J. M.; Moore, A. L.; Moore, T. A.; Gust, D. *J. Am. Chem. Soc.* **1995**, *177*, 7202.
(5) Kohler, B. E.; Spangler, C. W.; Westerfield, C. *J. Chem. Phys.* **1990**, *94*, 908.
(6) O'Neil, M. P.; Wasielewski, M. R.; Kakoled, M. M.; Kispert, L. D. *J. Chem. Phys.* **1991**, *95*, 7212.

(7) Slama-Schwok, A.; Blanchard-Desce, M.; Lehn, J.-M. *J. Phys. Chem.* **1990**, *94*, 3894.
(8) Lawson, J. M.; Paddon-Row, M. N.; Schuddeboom, W.; Warman, J. M.; Clayton, A. H. A.; Ghiggino, K. P. *J. Phys. Chem.* **1993**, *97*, 13099.
(9) Gaines III, G. L.; O'Neil, M. P.; Svec, W. A.; Niemczyk, M. P.; Wasielewski, M. R. *J. Am. Chem. Soc.* **1991**, *113*, 719.
(10) Penfield, K. W.; Miller, J. R.; Paddon-Row, M. N.; Cotsaris, E.; Oliver, A. M.; Hush, N. S. *J. Am. Chem. Soc.* **1987**, *109*, 5061.
(11) Jortner, J.; Bixon, M. *Ultrafast Phenomena VIII*; Springer Series in Chemical Physics, Springer: New York, 1993; Vol. 5.
(12) Gribi, P.; Isenmann, G.; Sigmund, E.; Quapil, G.; Holl, N.; Port, H. *J. Chem. Phys.* **1993**, *98*, 7969.
(13) Marcus, R. A. *J. Chem. Phys.* **1956**, *24*, 866.
(14) Marcus, R. A. *Discuss. Faraday Soc.* **1960**, *29*, 21.
(15) Marcus, R. A. *J. Phys. Chem.* **1963**, *67*, 853.
(16) Sutin, N. *Prog. Inorg. Chem.* **1981**, *30*, 441.
(17) Effenberger, F.; Niesert, C.-P. *Synthesis* **1992**, 1137.
(18) Hirsch, T.; Port, H.; Wolf, H. C. *Mol. Cryst. Liq. Cryst.* **1996**, *283*, 203.
(19) Maruszewska-Wieczorkowska, E.; Michalski, J. *Rocz. Chem.* **1964**, *38*, 625.
(20) Davidson, R. S.; Sheldon, R. A.; Trippet, S. *J. Chem. Soc. B* **1968**, 1700.
(21) Jones, W. J.; Stoicheff, B. P. *Phys. Rev. Lett.* **1964**, *13*, 657.
(22) Alfano, R. R.; Shapiro, S. L. *Chem. Phys. Lett.* **1971**, *8*, 631.
(23) Dick, B.; Hohlneicher, G. *Chem. Phys. Lett.* **1981**, *83*, 615.
(24) *CRC Handbook Series in organic Electrochemistry*; CRC Press: Cleveland, OH, 1977; Vol. 1.
(25) Rehm, D.; Weller, A. *Ber. Bunsenges. Phys. Chem.* **1969**, *73*, 834.
(26) Hirsch, T.; Port, H.; Wolf, H. C. to be published.
(27) Akiyama, K.; Tero-Kubota, S.; Ikegami, Y.; Ikenoue, T. *J. Phys. Chem.* **1985**, *89*, 339.
(28) Shida, T.; Kato, T. *Chem. Phys. Lett.* **1979**, *68*, 106.
(29) Sepiol, J. *J. Lumin.* **1986**, *36*, 115.
(30) Shida, T. *Physical Science Data*; Elsevier Science Publishers B. V.: New York, 1988; Vol. 34.
(31) Masnovi, J. M.; Huffman, J. C.; Kochi, J. K.; Hilinski, E. F.; Rentzepis, P. M. *Chem. Phys. Lett.* **1984**, *106*, 20.
(32) Fröhlich, H. *Theory of Dielectrics*; Oxford University Press: Oxford, U.K., 1958.
(33) Sumi, H.; Marcus, R. A. *J. Chem. Phys.* **1986**, *84*, 4272.
(34) Hubbard, J. B. *J. Chem. Phys.* **1978**, *68*, 1649.
(35) Simon, J. D. *Acc. Chem. Res.* **1988**, *21*, 128.
(36) Hubbard, J.; Onsager, L. *J. Chem. Phys.* **1977**, *67*, 4850.
(37) Barbara, P. F.; Jazerba, W. *Acc. Chem. Res.* **1988**, *21*, 195.
(38) Stratt, R. M.; Cho, M. *J. Chem. Phys.* **1994**, *100*, 6700.
(39) Ravichandran, S.; Bagchi, B. *Int. Rev. Phys. Chem.* **1995**, *14*, 271.
(40) Kosower, E. M.; Huppert, D. *Ann. Rev. Phys. Chem.* **1986**, *37*, 127.
(41) Englman, R.; Jortner, J. *Mol. Phys.* **1970**, *18*, 145.
(42) Kavarnos, G. J. *Topics in Current Chemistry*; Springer-Verlag: Berlin, 1990; Vol. 156.
(43) Landolt-Börnstein. *Optische Konstanten*; Springer: New York, 1962; Vol. II.